INTERNATIONAL JOURNAL FOR NUMERICAL METHODS IN FLUIDS, VOL. 9, 833–853 (1989)

INTERNAL WAVE REFLECTIONS AND TRANSMISSIONS ARISING FROM A NON-UNIFORM MESH. PART III: THE OCCURRENCE OF EVANESCENT WAVES IN THE CRANK–NICOLSON LINEAR FINITE ELEMENT SCHEME

B. CATHERS

NSW Public Works Department, Hydraulics Laboratory, 110B King Street, Manly Vale, NSW, Australia, 2093

S. BATES

British Gas Corporation, Engineering Research Station, Harvey Combe, Killingworth, PO Box 1LH, Newcastle upon Tyne NE99 1LH, U.K.

AND

B. A. O'CONNOR

Civil Engineering Department, Liverpool University, Brownlow Street, PO Box 147, Liverpool L69 3BX, U.K.

SUMMARY

The numerical scheme upon which this paper is based is the 1D Crank–Nicolson linear finite element scheme. In Part I of this series it was shown that for a certain range of incident wavelengths impinging on the interface of an expansion in nodal spacing, an evanescent (or spatially damped) wave results in the downstream region. Here in Part III an analysis is carried out to predict the wavelength and the spatial rate of damping for this wave. The results of the analysis are verified quantitatively with seven 'hot-start' numerical experiments and qualitatively with seven 'cold-start' experiments. Weare has shown that evanescent waves occur whenever the frequency of a disturbance at a boundary exceeds the maximum frequency given by the dispersion relation. In these circumstances the 'extended dispersion' relation can be used to determine the rate of spatial decay.

In the context of a domain consisting of two regions with different nodal spacings, the use of the group velocity concept shows that evanescent waves have no energy flux associated with them when energy is conserved.

KEY WORDS Fourier analysis Dispersion relation Reflected/transmitted evanescent waves Crank–Nicolson linear finite element scheme

1. INTRODUCTION

This series of papers is aimed at gaining a better fundamental understanding of the processes at work when numerical schemes are applied to non-uniform meshes.

Parts I and II were mainly concerned with the resulting waves which occur when an incident wave impinges on the interface of two regions with different nodal spacings.[1,2] The transmitted waves have real wave numbers. Under certain conditions of mesh *expansion*, however, it was shown that the transmitted waves could have complex wave numbers which corresponded to transmitted waves which were exponentially damped (or growing) in space. Such damped waves

0271–2091/89/070833–21$10.50

Received May 1988
Revised September 1988

are the subject of the present paper. It is implicit that the term 'damped' in this work stands for damped in space and not in time unless stated otherwise.

Throughout this work the subscripts 1 and 2 will refer to the upstream region 1 and the downstream region 2 respectively.

2. COMPLEX WAVE NUMBERS

When one incident wave or two incident waves with complementary wave numbers impinge on the interface between the two regions, it was shown in Part I, inequalities (22), that if the incident wavelength (L_1) was in the range

$$\frac{\pi}{\tan^{-1}\{\sqrt{3[H'+\sqrt{(H'^2-1)}]}\}} < \frac{L_1}{\Delta x_1} < \frac{\pi}{\tan^{-1}\{\sqrt{3[H'-\sqrt{(H'^2-1)}]}\}}, \qquad (1)$$

where $H' = \Delta x_2/\Delta x_1$, then the transmitted waves would have complex wave numbers (γ_2) which can be calculated from the dispersion relation. The inequality (1) is presented in Figure 1.

The dispersion relation is central to the analysis and there are two ways of using it. The two approaches are attributed to von Neumann and Weare and are schematized in Figure 2 using the dispersion relation.

In a von Neumann type of analysis, the (possibly) complex wave frequency (ω) is determined as a function of a real wave number (σ_r). For fully centred numerical schemes the wave frequency is always real. For non-centred schemes the wave frequency is complex and, depending upon the

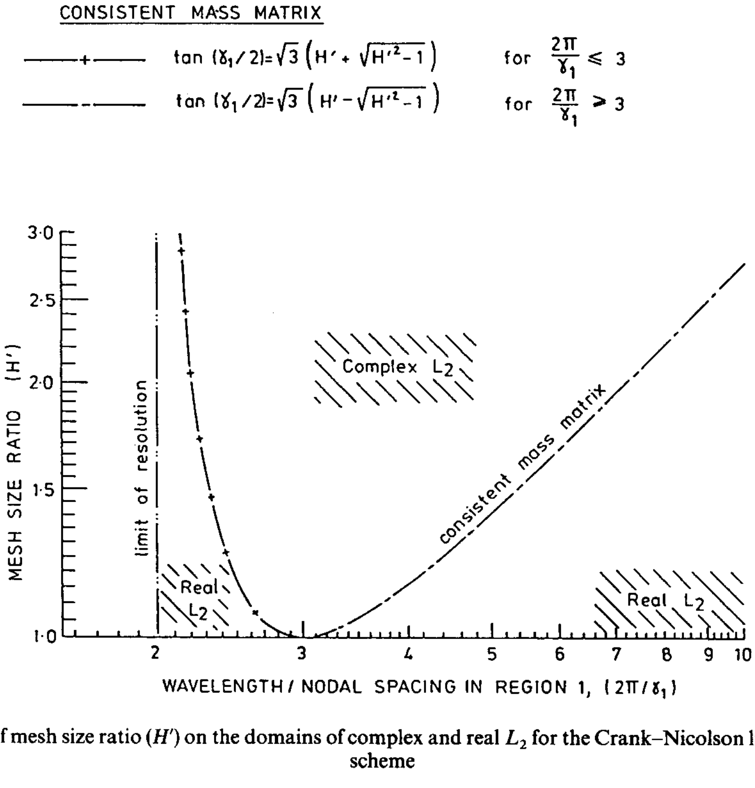

Figure 1. Effect of mesh size ratio (H') on the domains of complex and real L_2 for the Crank–Nicolson linear finite element scheme

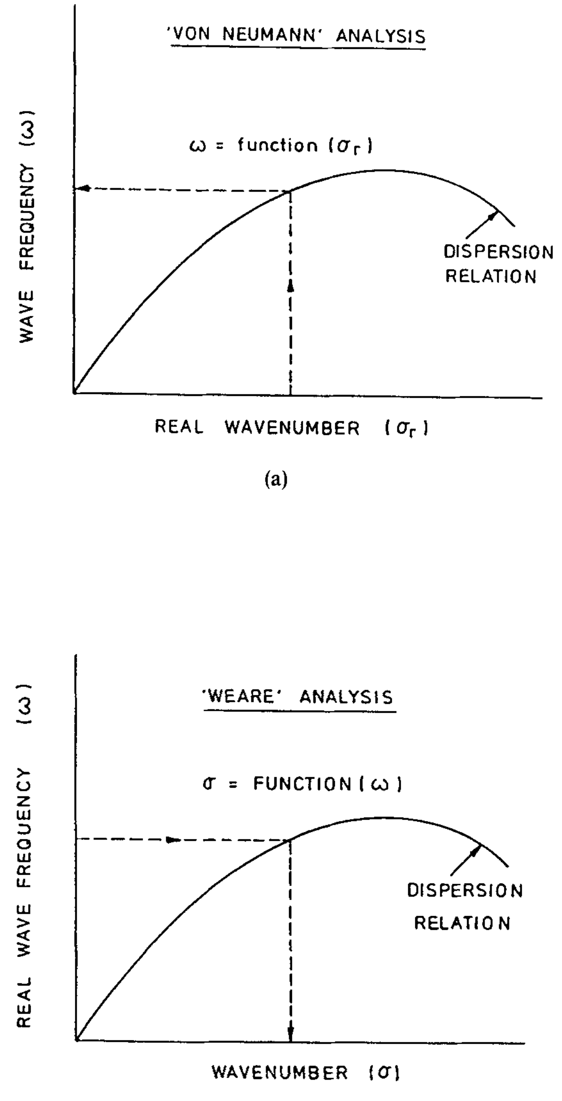

(a)

(b)

Figure 2. Temporal and spatial analyses using the dispersion relation ((a) and (b) respectively)

sign of the imaginary part, there will be either exponential growth or damping in *time* of the Fourier component(s). This approach is the basis of the von Neumann stability analysis.

Weare[3] was the first to address the alternative analysis in which the (possibly complex) wave number (σ) is determined as a function of a real wave frequency (ω_r) for fully centred schemes. Weare has also shown that a complex wave number corresponds to the exponential growth or damping in *space* of a Fourier wave component which is generated at an oscillating boundary. The applicability of the Weare analysis to the problem of mesh reflections can be seen if the interfacial node is viewed as the oscillating upstream boundary for region 2, which generates the transmitted wave also in region 2.

2.1. *'Extended' dispersion relation*

The dispersion relation for a numerical scheme is found from a von Neumann Fourier analysis. For the Crank–Nicolson linear finite element scheme at Courant number $\mathcal{C}$, the dispersion relation for a sinusoidal wave travelling in the $+x$-direction with dimensionless wave number $\gamma=\sigma\Delta x$ is well known and is given by

$$\tan\left(\frac{\omega\Delta t}{2}\right)=\frac{1{\cdot}5\mathcal{C}\sin\gamma}{2+\cos\gamma}. \tag{2}$$

In equation (2) it has only been necessary to consider waves with positive phase velocity (i.e. $\omega>0$), since it has already been shown in Part I[1] that no waves with negative phase velocity arise from the analysis.

For a given $\mathcal{C}$, the maximum wave frequency occurs at $\gamma=2\pi/3$, i.e.

$$\omega_{\max}\Delta t=2\tan^{-1}\left(\frac{\mathcal{C}\sqrt{3}}{2}\right). \tag{3}$$

By making recourse to the dispersion relation, it can be shown that when the frequency at an oscillating boundary exceeds the maximum value in equation (3), the wave number becomes complex. First we rearrange equation (2) to yield

$$\tan\left(\frac{\gamma}{2}\right)=\frac{1\pm\sqrt{(1-3R^2)}}{R}, \tag{4}$$

where

$$R=\left(\frac{2}{3\mathcal{C}}\right)\tan\left(\frac{\omega\Delta t}{2}\right). \tag{5}$$

Examination of the discriminant in equation (4) shows that γ will be complex whenever $R>1/\sqrt{3}$, i.e.

$$\tan\left(\frac{\omega\Delta t}{2}\right)>\frac{\mathcal{C}\sqrt{3}}{2}. \tag{6}$$

Incorporating equation (3) into the inequality (6), it is evident that γ is complex whenever ω exceeds $\omega_{\max}$, and γ is then given by

$$\tan\left(\frac{\gamma}{2}\right)=\frac{1\pm\mathrm{i}\sqrt{(1-3R^2)}}{R}.$$

The above expression is not amenable to evaluating the real and imaginary parts of γ because of the tan( ) function on the left-hand side. A simpler approach when γ is complex is to substitute $\gamma=\gamma_r+\mathrm{i}\gamma_i$ into the dispersion relation, equation (2):

$$\tan\left(\frac{\omega\Delta t}{2}\right)=\frac{1{\cdot}5\mathcal{C}\sin(\gamma_r+\mathrm{i}\gamma_i)}{2+\cos(\gamma_r+\mathrm{i}\gamma_i)},$$

i.e.

$$R=\frac{\sin(\gamma_r+\mathrm{i}\gamma_i)}{2+\cos(\gamma_r+\mathrm{i}\gamma_i)}=\frac{\sin\gamma_r\cosh\gamma_i+\mathrm{i}\cos\gamma_r\sinh\gamma_i}{2+\cos\gamma_r\cosh\gamma_i-\mathrm{i}\sin\gamma_r\sinh\gamma_i}, \tag{7}$$

i.e.

$$R(2+\cos\gamma_r\cosh\gamma_i)-\mathrm{i}R\sin\gamma_r\sinh\gamma_i=\sin\gamma_r\cosh\gamma_i+\mathrm{i}\cos\gamma_r\sinh\gamma_i.$$

This is a complex equation with two unknowns, γ_r and γ_i.

Equating the imaginary parts leads to

$$\sinh\gamma_i(\cos\gamma_r + R\sin\gamma_r) = 0,$$

i.e.

$$\gamma_i = 0 \quad \text{or} \quad \tan\gamma_r = -1/R,$$

and since γ is complex, $\gamma_i = 0$ can be discarded, leaving $\tan\gamma_r = -1/R$.

Equating the real parts leads to

$$R(2 + \cos\gamma_r\cosh\gamma_i) = \sin\gamma_r\cosh\gamma_i. \tag{8}$$

Since $\tan\gamma_r = -1/R$ and by taking cognisance of the quadrant, it is found that

$$\cos\gamma_r = \frac{-R}{\sqrt{(1+R^2)}}, \tag{9}$$

$$\sin\gamma_r = \frac{1}{\sqrt{(1+R^2)}}. \tag{10}$$

Substituting equations (9) and (10) into (8) gives

$$\cosh\gamma_i = \frac{2R}{\sqrt{(1+R^2)}}. \tag{11}$$

Therefore

$$\gamma = \gamma_r + i\gamma_i = \tan^{-1}\left(\frac{-1}{R}\right) + i\cosh^{-1}\left(\frac{2R}{\sqrt{(1+R^2)}}\right). \tag{12}$$

Since the cosh( ) function is even, its inverse admits both a positive and a negative value. If the solution of a dependent variable varies in time and space as

$$e^{i(\omega t - \sigma x)} = e^{i(\omega t - \sigma_r x)} e^{\sigma_i x},$$

where $\sigma = \sigma_r + i\sigma_i$, it is evident that the positive value of σ_i (or γ_i) corresponds to an exponentially growing Fourier component in the $+x$-direction, while the negative value corresponds to an exponentially damped wave in the $+x$-direction.

Equations (2) and (12) together are referred to as the 'extended dispersion relation' and have been plotted for the Courant numbers $\mathcal{C} = 0{\cdot}1$, 1, 10, 50 in Figure 3. Equation (2) is the ordinary dispersion relation, while equation (12) is its extension which permits the calculation of the real (σ_r) and imaginary (σ_i) components of the wave number when $\omega_{\max}$ is exceeded at a boundary. Figure 3 shows the variation of the real and imaginary parts of the wave number with Courant number and angular frequency, and how the extension to complex wave numbers (i.e. short dashes in the figure) fits in with the ordinary dispersion relation.

2.2. Calculation of the complex wave numbers in different regions

We now return to the situation in which the 1D domain consists of two regions 1 and 2 which are *physically* identical (i.e. same depth and same fluid) but which are (*computationally*) discernible only on the basis of having different nodal spacings (i.e. Δx_1 and Δx_2).

In Section 2.1 it was shown that it is possible under certain operating conditions to get complex wave numbers in either or both of the two regions. Attention is now focused on those situations where the wave numbers are complex in just region 2.

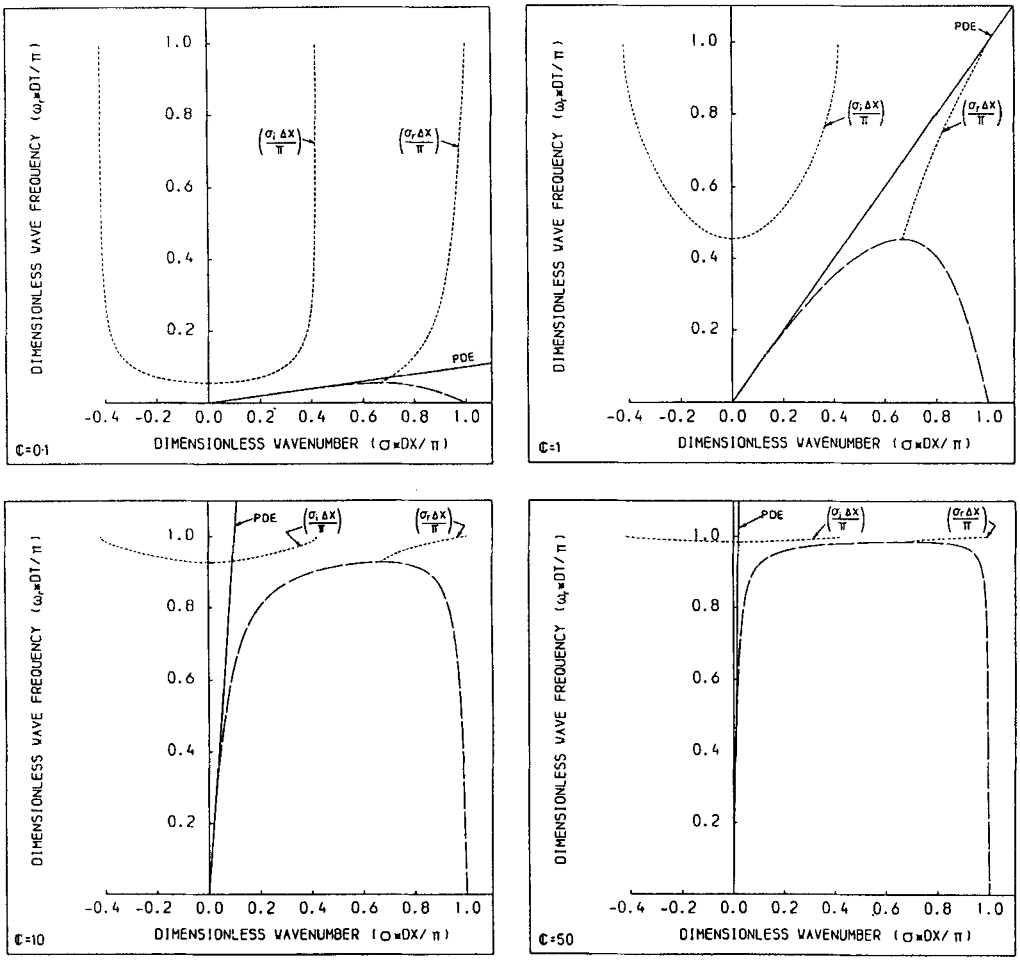

Figure 3. Extended dispersion relation for the Crank–Nicolson linear finite element scheme at Courant Numbers $\mathcal{C}=0{\cdot}1$, 1·0, 10·0, 50·0 (left to right)

2.2.1. Solving for complex γ_2 in terms of real γ_1. In the case of a mesh expansion, it has been shown in Section 3.3 of Part I that γ_2 can be complex $(=\gamma_r+i\gamma_i)$ and γ_1 real. The situation is depicted in Figures 4(a) and 4(b). In region 1 the complementary real wave numbers are denoted by σ_A and σ_B. In region 2 the two complex wave numbers correspond to waves which grow (i.e. $\sigma_r+i\sigma_i$) or decay (i.e. $\sigma_r-i\sigma_i$) exponentially with space away from the origin (see Figure 4(a)). The dispersion relations for the two regions in Figure 4(b) show how the real components of the two complex wave numbers are the same but the imaginary parts are equal but opposite in sign. The incident waves *A* and *B* have real wave numbers since the wave frequency (ω) is less than $\omega_{\max}$ for region 1. The wave numbers in region 2 are complex because ω is greater than $\omega_{\max}$ in

$$\omega_{\max}=\left(\frac{2}{\Delta t}\right)\tan^{-1}\left(\frac{\mathcal{C}_2\sqrt{3}}{2}\right)$$

(from equation (3)). The two complex γ_2 values will now be found in terms of real γ_1, which can refer to either of the two complementary wave numbers in region 1, viz. $\gamma_A=\sigma_A\Delta x_1$ or $\gamma_B=\sigma_B\Delta x_1$ in Figure 4.

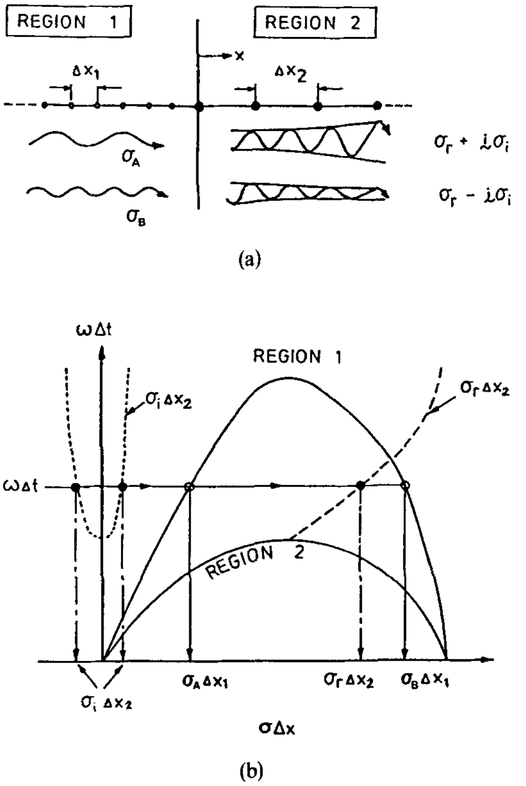

Figure 4. The occurrence of complex wavenumbers due to a mesh expansion. (a) Waves present in the system for a *mesh expansion*—the wavenumbers present in Region1 are real while those in Region 2 are complex conjugates. (b) Schematics of the dispersion relation for Region 1 and the extended dispersion relation for Region 2 for A *mesh expansion*

From the dispersion relation for the two regions,

$$\tan\left(\frac{\omega\Delta t}{2}\right)=\frac{1{\cdot}5\not{C}_1\sin\gamma_1}{2+\cos\gamma_1}=\frac{1{\cdot}5\not{C}_2\sin(\gamma_r+i\gamma_i)}{2+\cos(\gamma_r+i\gamma_i)},$$

where $\gamma_2=\gamma_r+i\gamma_i$ and $\gamma_1=2\pi/(L_1/\Delta x_1)$; i.e.

$$R_1=\frac{\sin(\gamma_r+i\gamma_i)}{2+\cos(\gamma_r+i\gamma_i)},$$

where

$$R_1=\left(\frac{2}{3\not{C}_2}\right)\tan\left(\frac{\omega\Delta t}{2}\right)=\frac{H'\sin\gamma_1}{2+\cos\gamma_1} \tag{13}$$

and $H'=\Delta x_2/\Delta x_1$.

The solution for γ_2 is similar to that for equation (12) and is

$$\gamma_2=\gamma_r+i\gamma_i=\tan^{-1}\left(\frac{-1}{R_1}\right)+i\cosh^{-1}\left(\frac{2R_1}{\sqrt{(1+R_1^2)}}\right). \tag{14}$$

The case in which complex γ_1 is found in terms of real γ_2 is of less interest than finding complex γ_2 in terms of real γ_1. This is because the incident wave is exponentially growing or damped in space. However, this is not to say that this situation is unlikely to be met in practice, because it may well occur where a mesh expansion is followed by a mesh refinement.

It is the *real* part of the wave number which determines the wavelength(s) of the transmitted wave(s). Since the real part of the transmitted wave number in equation (14) is the same irrespective of the imaginary part, it is clear that the wavelengths of the growing and damped transmitted waves are equal. (By combining the real part of equation (14) with the last part of equation (13) for R_1, it is possible to relate the wavelength in region 1 ($L_1=2\pi/\gamma_1$) to the wavelength in region 2 ($L_2=2\pi/\gamma_r$)—see the dashed line in Figure 3 of Part I.) The inverse tan( ) function is multivalued, but only one of these values corresponds to a resolvable wavelength, which must be greater than $2\Delta x_2$.

These points are best illustrated by an example. All the numerical experiments with a mesh expansion had a mesh size ratio of $H'=2$. From inequality (1) this means that any incident waves with wavelengths between $2{\cdot}2166\Delta x_1$ and $7{\cdot}2301\Delta x_1$ would give rise to waves in region 2, which had complex wave numbers. Consider a $4\Delta x_1$ incident wave. From equation (14) the wave numbers of any transmitted waves would be

$$\gamma_2=\tan^{-1}\left(\frac{-1}{1}\right)+\mathrm{i}\cosh^{-1}\left(\frac{2\times 1}{\sqrt{(1+1^2)}}\right)$$

$$=3\pi/4,\ 7\pi/4,\ 11\pi/4,\ 15\pi/4\ldots\pm\mathrm{i}(0{\cdot}8814).$$

The real part of γ_2 corresponds to wavelengths of $(8/3)\Delta x_2$, $(8/7)\Delta x_2$, $(8/11)\Delta x_2$, $(8/15)\Delta x_2\ldots$ and only the first value is taken since it is the only resolvable wavelength. If the exponentially growing wave is present it will amplify at the rate of $\exp(\sigma_i x)=\exp(0{\cdot}8814x/\Delta x_2)$, and if the damped wave is present it will decay at the rate of $\exp(-0{\cdot}8814x/\Delta x_2)$ in the positive x-direction. With this information on complex wave numbers, it is now possible to solve for the wave amplitudes.

3. REFLECTION/TRANSMISSION ANALYSIS DUE TO A CHANGE IN MESH SIZE

The assumed wave configuration consists of two incident waves (A and B) with real complementary wave numbers in region 1 and a single spatially damped, evanescent transmitted wave (C) in region 2. The case with the damped wave was selected because it did not involve an exponentially growing wave in region 2 and was therefore amenable to verification by numerical experiments and, owing to the downstream boundary condition, is the more likely to occur. The amplitude of the surface elevation at the interfacial node is again denoted by α.

The convention for labelling the two incident waves A and B is the same as was used in Part II, i.e. wave A refers to the 'long' incident wave with a positive group velocity (i.e. $L_A\geqslant 3\Delta x_1$) and wave B refers to its 'short'-wavelength complement (i.e. $L_B\leqslant 3\Delta x_1$) which has a negative group velocity.

In region 1, where $x<0$, the instantaneous surface elevation and velocity are given by

$$\eta(x,t)=A\mathrm{e}^{\mathrm{i}(\omega t-\sigma_A x)}+B\mathrm{e}^{\mathrm{i}(\omega t-\sigma_B x)}, \tag{15}$$

$$u(x,t)=\sqrt{(g/h)}\,\eta(x,t); \tag{16}$$

in region 2, where $x>0$, they are

$$\eta(x,t)=C\mathrm{e}^{\mathrm{i}(\omega t-\sigma_C x)}, \tag{17}$$

$$u(x,t)=\sqrt{(g/h)}\,\eta(x,t), \tag{18}$$

where σ_A and σ_B are the real wave numbers of waves A and B, and σ_C is the complex wavenumber of evanescent wave C; and at the interfacial node, where $x=0$, they are

$$\eta(0, t)=\alpha e^{i\omega t}, \tag{19}$$

$$u(0, t)=\sqrt{(g/h)}\,\eta(0, t). \tag{20}$$

Application of the Crank–Nicolson linear finite element method centred about $x=0$ to the momentum equation (see equation (29) of Part I) gives

$$\frac{\Delta x_1}{6}\left[\left(\frac{u^{n+1}-u^n}{\Delta t}\right)_{-1}+2\left(\frac{u^{n+1}-u^n}{\Delta t}\right)_0\right]+\frac{\Delta x_2}{6}\left[2\left(\frac{u^{n+1}-u^n}{\Delta t}\right)_0+\left(\frac{u^{n+1}-u^n}{\Delta t}\right)_1\right]$$
$$+\frac{g}{2}\left(\frac{\eta_1-\eta_{-1}}{\Delta x}\right)^{n+1}+\frac{g}{2}\left(\frac{\eta_1-\eta_{-1}}{\Delta x}\right)^n=0. \tag{21}$$

Substitution of equations (15)–(20) into the appropriate terms in equation (21) yields

$$A\left[\frac{1}{6\not{C}_1}\left(\frac{\lambda-1}{\lambda+1}\right)e^{i\gamma_A}-\frac{1}{4}e^{i\gamma_A}\right]+B\left[\frac{1}{6\not{C}_1}\left(\frac{\lambda-1}{\lambda+1}\right)e^{i\gamma_B}-\frac{1}{4}e^{i\gamma_B}\right]$$
$$+\alpha\left[\frac{1}{3}\left(\frac{\lambda-1}{\lambda+1}\right)\left(\frac{1}{\not{C}_1}+\frac{1}{\not{C}_2}\right)+C\biggl(\frac{1}{6\not{C}_2}\left(\frac{\lambda-1}{\lambda+1}\right)e^{i\gamma_C}+\frac{1}{4}e^{i\gamma_C}\right]=0, \tag{22}$$

where

$$\lambda=e^{i\omega\Delta t},\qquad \gamma_A=\sigma_A\Delta x_1,\qquad \gamma_B=\sigma_B\Delta x_1,\qquad \gamma_C=\sigma_C\Delta x_2.$$

Since equations (15), (17) and (19) must be compatible at $x=0$ for all times,

$$A+B=\alpha=C. \tag{23}$$

Also, since the angular frequency ω is the same in both regions, we have from the dispersion relation (equation (2))

$$\frac{\lambda-1}{\lambda+1}=i\left(\frac{1{\cdot}5\not{C}_1\sin\gamma_A}{2+\cos\gamma_A}\right)=i\left(\frac{1{\cdot}5\not{C}_1\sin\gamma_B}{2+\cos\gamma_B}\right)=i\left(\frac{1{\cdot}5\not{C}_2\sin\gamma_C}{2+\cos\gamma_C}\right). \tag{24}$$

Insertion of equations (23) and (24) into (22) to eliminate α, C and λ and then simplifying leads to

$$B=A\left[\frac{E_A-E_C}{-E_B+E_C}\right], \tag{25}$$

where

$$E_A=\frac{1+2\cos\gamma_A}{2+\cos\gamma_A}=-E_B,\qquad E_B=\frac{1+2\cos\gamma_B}{2+\cos\gamma_B}, \tag{26}$$

$$E_C=\frac{1+2\cos\gamma_C}{2+\cos\gamma_C}. \tag{27}$$

Therefore from equations (23) and (25)–(27) the solutions are

$$B=A\left[\frac{E_A-E_C}{E_A+E_C}\right], \tag{28}$$

$$C=2A\left[\frac{E_A}{E_A+E_C}\right], \tag{29}$$

where γ_A is real,

$$\gamma_C = \tan^{-1}\left(\frac{-1}{R_A}\right) + i\cosh^{-1}\left(\frac{2R_A}{\sqrt{(1+R_A^2)}}\right) \quad \text{(from equation (14))}, \tag{30}$$

$$R_A = \frac{H'\sin\gamma_A}{2+\cos\gamma_A} \quad \text{(from equation (13))}. \tag{31}$$

Thus for an incident wave A with a real amplitude, the second incident wave (B) has complex amplitude but real wave number, and the transmitted evanescent wave (C) has complex amplitude and complex wave number. (It will be evident from equation (34) that a complex wave amplitude implies a phase lag or lead with respect to the incident wave.)

The modulus of the amplitude of the transmitted wave, $|C|$, resulting from a unit incident wave ($A=1$) is given by equation (29) and is plotted as a finely dashed line in Figures 5–7 of Part I, where $|C|$ is equal to $|\tau_1| = |\tau_2|$.

4. 'HOT-START' NUMERICAL EXPERIMENTS

The numerical model used to check the analysis was based upon the linear shallow water equations

$$\frac{\partial u}{\partial t} + g\frac{\partial \eta}{\partial x} = 0, \tag{32}$$

$$\frac{\partial \eta}{\partial t} + h\frac{\partial u}{\partial x} = 0. \tag{33}$$

Seven numerical experiments were carried out with incident wavelengths for wave A varying between $3{\cdot}0\Delta x_1$ and $7{\cdot}23\Delta x_1$. This range was selected in order to give rise to a damped wave in region 2 (see Section 3.3 of Part I), as well as having an incident wave (A) with a positive group velocity. Both waves A and B are incident in terms of phase velocity but only wave A is incident in terms of group velocity.

The initial conditions were as follows. In region 1 and at the interface ($x \leqslant 0$),

$$\eta(x,t) = Ae^{i(\omega t - \sigma_A x)} + |B|e^{i\arg B}\,e^{i(\omega t - \sigma_B x)}, \tag{34}$$

$$u(x,t) = \eta(x,t)\sqrt{(g/h)}, \tag{35}$$

and in region 2 and at the interface ($x \geqslant 0$),

$$\begin{aligned}\eta(x,t) &= |C|e^{i\arg C}\,e^{i(\omega t - \sigma_C x)}\\ &= |C|e^{i\arg C}\,e^{i[\omega t - \mathrm{Re}(\sigma_C)x]}\,e^{\mathrm{Im}(\sigma_C)x},\end{aligned} \tag{36}$$

$$u(x,t) = \eta(x,t)\sqrt{(g/h)}, \tag{37}$$

where

A, σ_A were data and are real
B was defined by equation (28) and is complex
$\sigma_B = \gamma_B/\Delta x_1$ is real and was related to σ_A by the equation

$$\tan(\gamma_A/2)\tan(\gamma_B/2) = 3 \tag{38}$$

(see equation (20) of Part II)

C is complex and was defined by equation (29)
$\sigma_C = \gamma_C/\Delta x_2$ is complex and was defined by equation (30)
Re( ) and Im( ) denote the real and imaginary parts.

Thus, once the details of wave A are known, equations (34)–(37) could then be used to set up the initial conditions. As for previous tests in Parts I and II, the numerical model was run for some duration starting with the initial conditions and output was obtained at two later times.

4.1. 'Hot-start' data used in the numerical experiments

A mesh size ratio of $H' = 2$ was used in all seven tests. Tests 1–7 correspond to decreasing spatial damping of wave C. The data are contained in Table I.

4.2. Results and conclusions from the 'hot-start' numerical experiments

The results for the seven tests are contained in Figures 5(a)–11(a). It is clear that in each case the analysis matches the results from the numerical model since the differences between the two, which are denoted by a small triangle, are all zero at all times.

From test 1 to test 7 the wavelength of wave A was progressively increased from $3{\cdot}0\Delta x_1$ to $7{\cdot}23\Delta x_1$. In the first test the two incident waves both had a $3{\cdot}0\Delta x_1$ wavelength and were π radians out of phase with each other, and therefore annihilated each other (see Figure 5(a)). In the second test (see Figure 6(a)) wave A (which had a real amplitude) had its wavelength increased to $3{\cdot}01\Delta x_1$, while wave B (which had a complex amplitude) had its wavelength reduced to $2{\cdot}99\Delta x_1$. When these two waves were superimposed, there was only the slightest discernible disturbance at the upstream end of region 2.

Figure 7(a) contains the results of the third test in which the presence of a spatially damped wave in region 2 is easily noticeable. The wavelength of wave A was now $4{\cdot}0\Delta x_1$. Figures 8(a)–11(a) contain the results of tests 4–7 and the progression from a heavily damped wave in region 2 to a very lightly damped wave is clear. The amount of spatial damping in wave C is dictated by the term $e^{\mathrm{Im}(\sigma_C)x} = e^{\{\mathrm{Im}(\gamma_C)/\Delta x_2\}x}$ in equation (36), where γ_C has been included in Table I below. It is seen that the maximum damping occurred in test 1 and the least damping was present in test 7.

With the results of the analysis verified, a parallel series of tests was undertaken, but this time a 'cold-start' was used.

5. 'COLD-START' NUMERICAL EXPERIMENTS

In the 'cold-start' numerical experiments the initial conditions were specified by equations (34) and (35) for $x \leqslant 0$. For $x > 0$ both the surface elevation and the velocity were set to zero. The Crank–Nicolson linear finite element model was used to predict the water levels and velocities at subsequent times. The data for the initial conditions which were used in the 'cold-start' tests will not be listed separately since they are already contained in Table I for the previous set of tests, with the only difference being that the complex wave amplitudes B and C were set to zero. The only wave data required were the wave amplitude ($A = 1$) and the wavelength (L_A).

5.1. Results and conclusions of the 'cold-start' numerical experiments

The output from the seven 'cold-start' experiments is displayed in Figures 5(b)–11(b) below the corresponding 'hot' start tests of Section 4. In Figure 5(b) it is evident that in spite of a positive *phase velocity*, the incident $3\Delta x_1$ waves in region 1 have been unable to penetrate region 2. A small

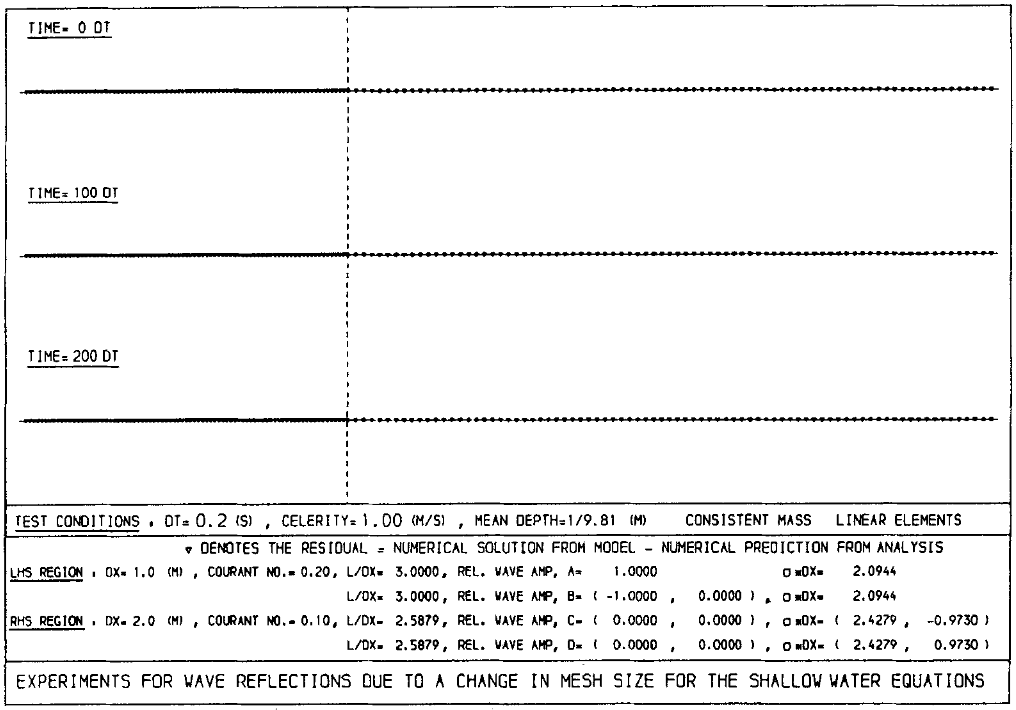

```
TEST CONDITIONS , DT= 0.2 (S) , CELERITY= 1.00 (M/S) , MEAN DEPTH=1/9.81 (M)     CONSISTENT MASS   LINEAR ELEMENTS
                   ▼ DENOTES THE RESIDUAL = NUMERICAL SOLUTION FROM MODEL - NUMERICAL PREDICTION FROM ANALYSIS
LHS REGION , DX= 1.0 (M) , COURANT NO.= 0.20, L/DX= 3.0000, REL. WAVE AMP, A=    1.0000                σ*DX=   2.0944
                                              L/DX= 3.0000, REL. WAVE AMP, B= ( -1.0000 ,   0.0000 ) , σ*DX=   2.0944
RHS REGION , DX= 2.0 (M) , COURANT NO.= 0.10, L/DX= 2.5879, REL. WAVE AMP, C= (  0.0000 ,   0.0000 ) , σ*DX= ( 2.4279 ,  -0.9730 )
                                              L/DX= 2.5879, REL. WAVE AMP, D= (  0.0000 ,   0.0000 ) , σ*DX= ( 2.4279 ,   0.9730 )
EXPERIMENTS FOR WAVE REFLECTIONS DUE TO A CHANGE IN MESH SIZE FOR THE SHALLOW WATER EQUATIONS
```

Figure 5(a). Hot start numerical experiment—waves present: incident waves A ($3{\cdot}0000\Delta x_1$) and B ($3{\cdot}0000\Delta x_1$)

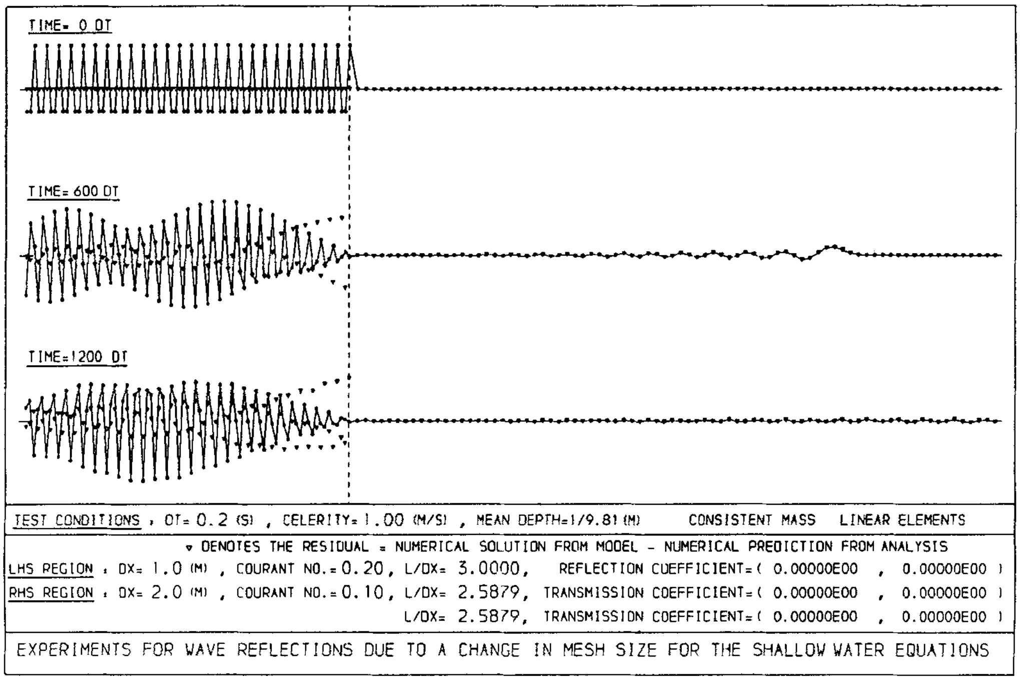

```
TEST CONDITIONS , DT= 0.2 (S) , CELERITY= 1.00 (M/S) , MEAN DEPTH=1/9.81 (M)      CONSISTENT MASS   LINEAR ELEMENTS
                   ▼ DENOTES THE RESIDUAL = NUMERICAL SOLUTION FROM MODEL - NUMERICAL PREDICTION FROM ANALYSIS
LHS REGION : DX= 1.0 (M) , COURANT NO.= 0.20, L/DX= 3.0000,   REFLECTION COEFFICIENT= ( 0.00000E00  ,  0.00000E00 )
RHS REGION : DX= 2.0 (M) , COURANT NO.= 0.10, L/DX= 2.5879, TRANSMISSION COEFFICIENT= ( 0.00000E00  ,  0.00000E00 )
                                              L/DX= 2.5879, TRANSMISSION COEFFICIENT= ( 0.00000E00  ,  0.00000E00 )
EXPERIMENTS FOR WAVE REFLECTIONS DUE TO A CHANGE IN MESH SIZE FOR THE SHALLOW WATER EQUATIONS
```

Figure 5(b). Cold start numerical experiment with initially only the incident waves A ($3{\cdot}0000\Delta x_1$) present

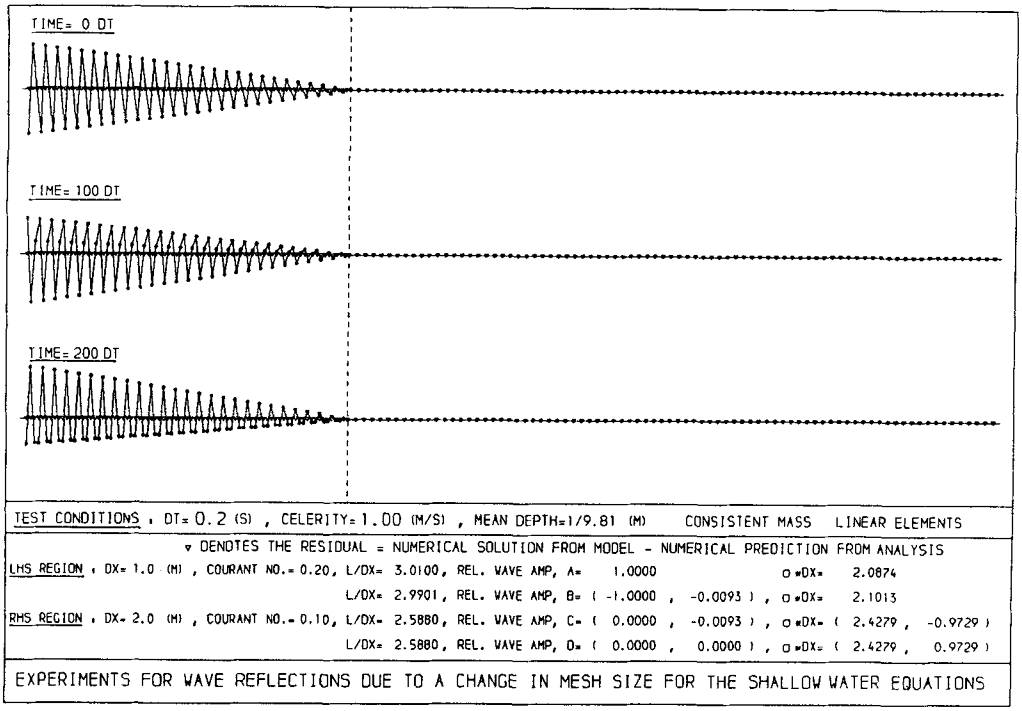

```
TEST CONDITIONS , DT= 0.2 (S) , CELERITY= 1.00 (M/S) , MEAN DEPTH=1/9.81 (M)    CONSISTENT MASS   LINEAR ELEMENTS
               ▼ DENOTES THE RESIDUAL = NUMERICAL SOLUTION FROM MODEL - NUMERICAL PREDICTION FROM ANALYSIS
LHS REGION , DX= 1.0 (M) , COURANT NO.= 0.20, L/DX= 3.0100, REL. WAVE AMP, A=   1.0000                σ *DX=  2.0874
                                              L/DX= 2.9901, REL. WAVE AMP, B= ( -1.0000 , -0.0093 ) , σ *DX=  2.1013
RHS REGION , DX= 2.0 (M) , COURANT NO.= 0.10, L/DX= 2.5880, REL. WAVE AMP, C= (  0.0000 , -0.0093 ) , σ *DX= ( 2.4279 , -0.9729 )
                                              L/DX= 2.5880, REL. WAVE AMP, D= (  0.0000 ,  0.0000 ) , σ *DX= ( 2.4279 ,  0.9729 )
EXPERIMENTS FOR WAVE REFLECTIONS DUE TO A CHANGE IN MESH SIZE FOR THE SHALLOW WATER EQUATIONS
```

Figure 6(a). Hot start numerical experiment—waves present: incident waves A ($3{\cdot}0100\Delta x_1$) and B ($2{\cdot}9901\Delta x_1$), and damped transmitted wave C

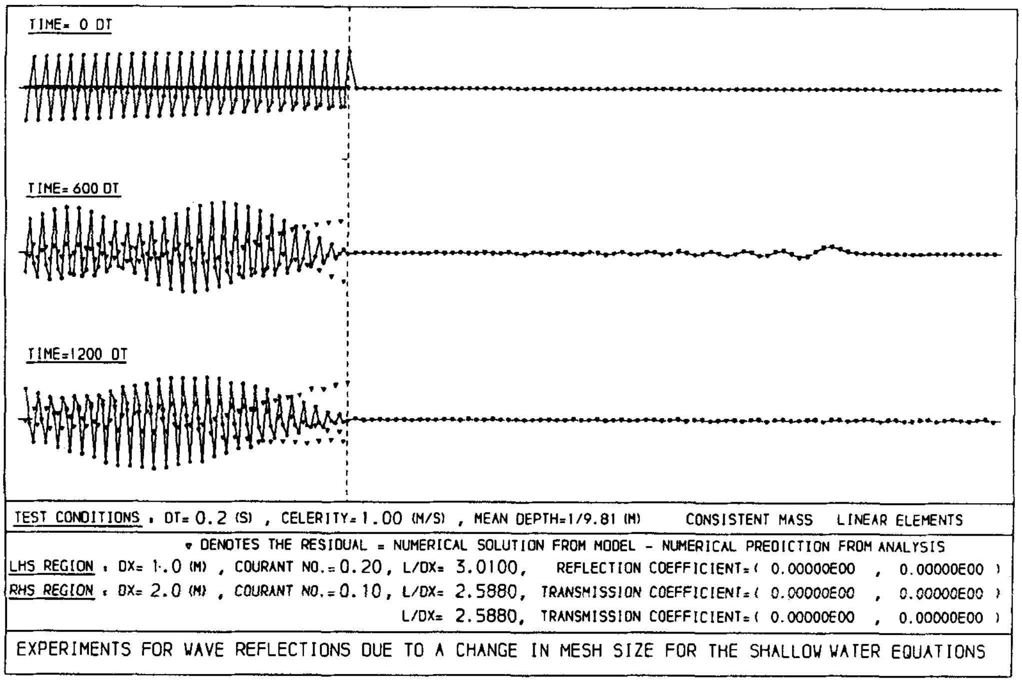

```
TEST CONDITIONS , DT= 0.2 (S) , CELERITY= 1.00 (M/S) , MEAN DEPTH=1/9.81 (M)    CONSISTENT MASS   LINEAR ELEMENTS
               ▼ DENOTES THE RESIDUAL = NUMERICAL SOLUTION FROM MODEL - NUMERICAL PREDICTION FROM ANALYSIS
LHS REGION , DX= 1.0 (M) , COURANT NO.= 0.20, L/DX= 3.0100,  REFLECTION COEFFICIENT= ( 0.00000E00 , 0.00000E00 )
RHS REGION , DX= 2.0 (M) , COURANT NO.= 0.10, L/DX= 2.5880, TRANSMISSION COEFFICIENT= ( 0.00000E00 , 0.00000E00 )
                                              L/DX= 2.5880, TRANSMISSION COEFFICIENT= ( 0.00000E00 , 0.00000E00 )
EXPERIMENTS FOR WAVE REFLECTIONS DUE TO A CHANGE IN MESH SIZE FOR THE SHALLOW WATER EQUATIONS
```

Figure 6(b). Cold start numerical experiment with initially only the incident waves A ($3{\cdot}0000\Delta x_1$) present

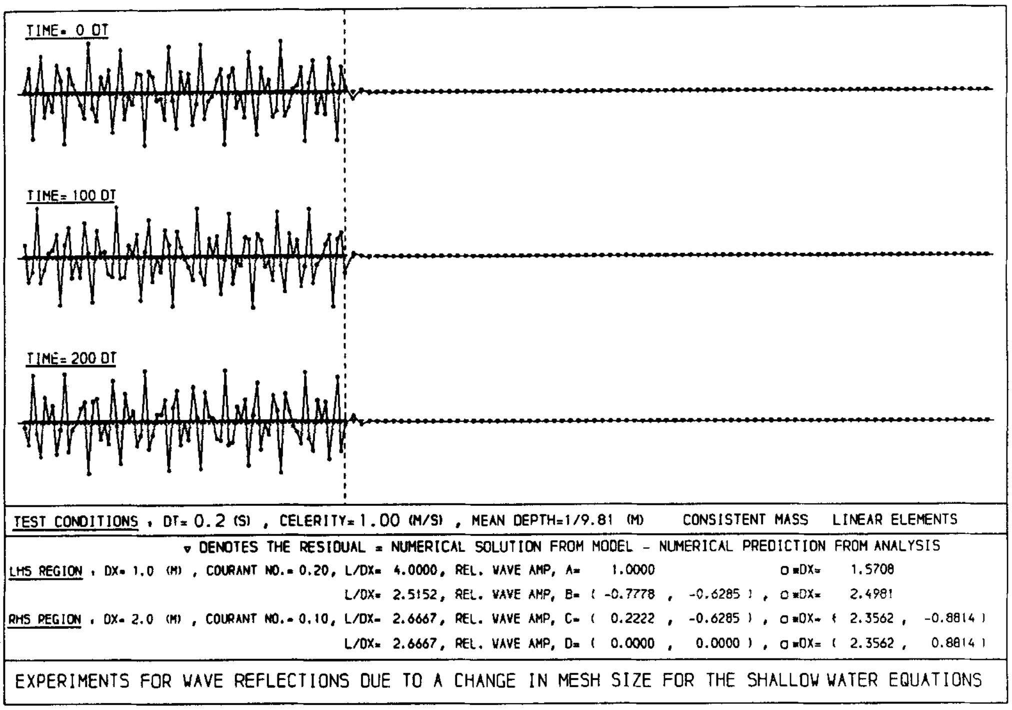

TEST CONDITIONS , DT= 0.2 (S) , CELERITY= 1.00 (M/S) , MEAN DEPTH=1/9.81 (M) CONSISTENT MASS LINEAR ELEMENTS

▾ DENOTES THE RESIDUAL = NUMERICAL SOLUTION FROM MODEL - NUMERICAL PREDICTION FROM ANALYSIS
LHS REGION , DX= 1.0 (M) , COURANT NO.= 0.20, L/DX= 4.0000, REL. WAVE AMP, A= 1.0000 σ*DX= 1.5708
L/DX= 2.5152, REL. WAVE AMP, B= (-0.7778 , -0.6285) , σ*DX= 2.4981
RHS REGION , DX= 2.0 (M) , COURANT NO.= 0.10, L/DX= 2.6667, REL. WAVE AMP, C= (0.2222 , -0.6285) , σ*DX= (2.3562 , -0.8814)
L/DX= 2.6667, REL. WAVE AMP, D= (0.0000 , 0.0000) , σ*DX= (2.3562 , 0.8814)

EXPERIMENTS FOR WAVE REFLECTIONS DUE TO A CHANGE IN MESH SIZE FOR THE SHALLOW WATER EQUATIONS

Figure 7(a). Hot start numerical experiment—waves present: incident waves A ($4{\cdot}0000\Delta x_1$) and B ($2{\cdot}5152\Delta x_1$), and damped transmitted wave C

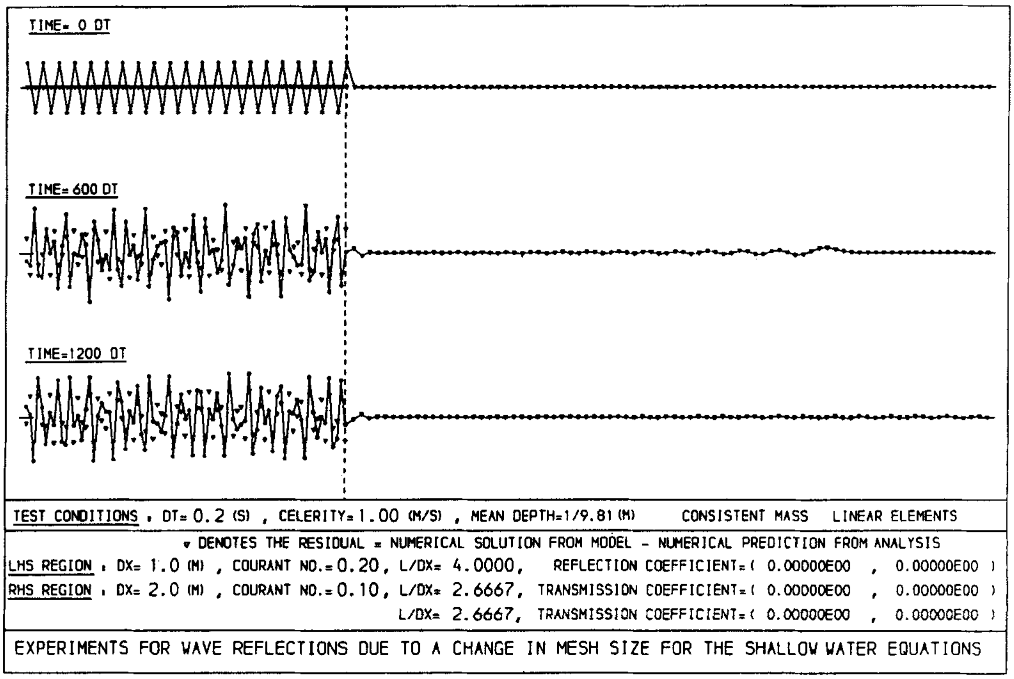

TEST CONDITIONS , DT= 0.2 (S) , CELERITY= 1.00 (M/S) , MEAN DEPTH=1/9.81 (M) CONSISTENT MASS LINEAR ELEMENTS

▾ DENOTES THE RESIDUAL = NUMERICAL SOLUTION FROM MODEL - NUMERICAL PREDICTION FROM ANALYSIS
LHS REGION , DX= 1.0 (M) , COURANT NO.= 0.20, L/DX= 4.0000, REFLECTION COEFFICIENT= (0.00000E00 , 0.00000E00)
RHS REGION , DX= 2.0 (M) , COURANT NO.= 0.10, L/DX= 2.6667, TRANSMISSION COEFFICIENT= (0.00000E00 , 0.00000E00)
L/DX= 2.6667, TRANSMISSION COEFFICIENT= (0.00000E00 , 0.00000E00)

EXPERIMENTS FOR WAVE REFLECTIONS DUE TO A CHANGE IN MESH SIZE FOR THE SHALLOW WATER EQUATIONS

Figure 7(b). Cold start numerical experiment with initially only the incident waves A ($4{\cdot}0000\Delta x_1$) present

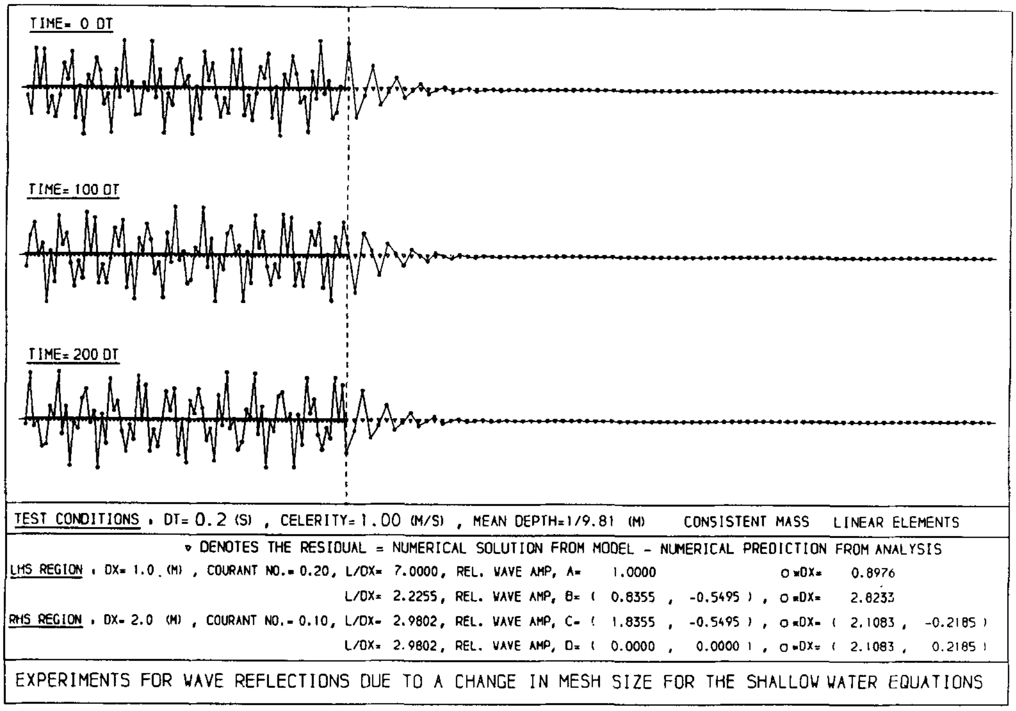

```
TEST CONDITIONS , DT= 0.2 (S) , CELERITY= 1.00 (M/S) , MEAN DEPTH=1/9.81 (M)     CONSISTENT MASS   LINEAR ELEMENTS
                   ▿ DENOTES THE RESIDUAL = NUMERICAL SOLUTION FROM MODEL - NUMERICAL PREDICTION FROM ANALYSIS
LHS REGION , DX= 1.0 (M) , COURANT NO.= 0.20, L/DX= 7.0000, REL. WAVE AMP, A=   1.0000                  σ*DX=   0.8976
                                              L/DX= 2.2255, REL. WAVE AMP, B= ( 0.8355 ,  -0.5495 ) , σ*DX=   2.8233
RHS REGION , DX= 2.0 (M) , COURANT NO.= 0.10, L/DX= 2.9802, REL. WAVE AMP, C= ( 1.8355 ,  -0.5495 ) , σ*DX= ( 2.1083 ,  -0.2185 )
                                              L/DX= 2.9802, REL. WAVE AMP, D= ( 0.0000 ,   0.0000 ) , σ*DX= ( 2.1083 ,   0.2185 )
EXPERIMENTS FOR WAVE REFLECTIONS DUE TO A CHANGE IN MESH SIZE FOR THE SHALLOW WATER EQUATIONS
```

Figure 8(a). Hot start numerical experiment—waves present: incident waves A ($7{\cdot}0000\Delta x_1$) and B ($2{\cdot}2255\Delta x_1$), and damped transmitted wave C

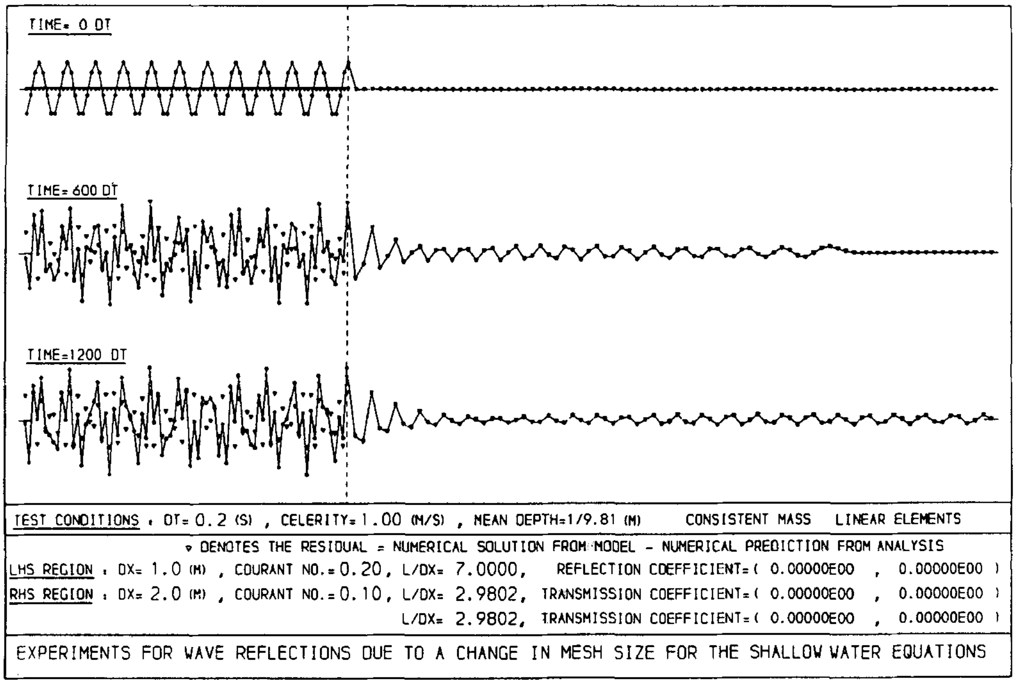

```
TEST CONDITIONS , DT= 0.2 (S) , CELERITY= 1.00 (M/S) , MEAN DEPTH=1/9.81 (M)     CONSISTENT MASS   LINEAR ELEMENTS
                   ▿ DENOTES THE RESIDUAL = NUMERICAL SOLUTION FROM MODEL - NUMERICAL PREDICTION FROM ANALYSIS
LHS REGION : DX= 1.0 (M) , COURANT NO.= 0.20, L/DX= 7.0000,   REFLECTION COEFFICIENT= ( 0.00000E00  ,  0.00000E00 )
RHS REGION : DX= 2.0 (M) , COURANT NO.= 0.10, L/DX= 2.9802, TRANSMISSION COEFFICIENT= ( 0.00000E00  ,  0.00000E00 )
                                              L/DX= 2.9802, TRANSMISSION COEFFICIENT= ( 0.00000E00  ,  0.00000E00 )
EXPERIMENTS FOR WAVE REFLECTIONS DUE TO A CHANGE IN MESH SIZE FOR THE SHALLOW WATER EQUATIONS
```

Figure 8(b). Cold start numerical experiment with initially only the incident waves A ($7{\cdot}0000\Delta x_1$) present

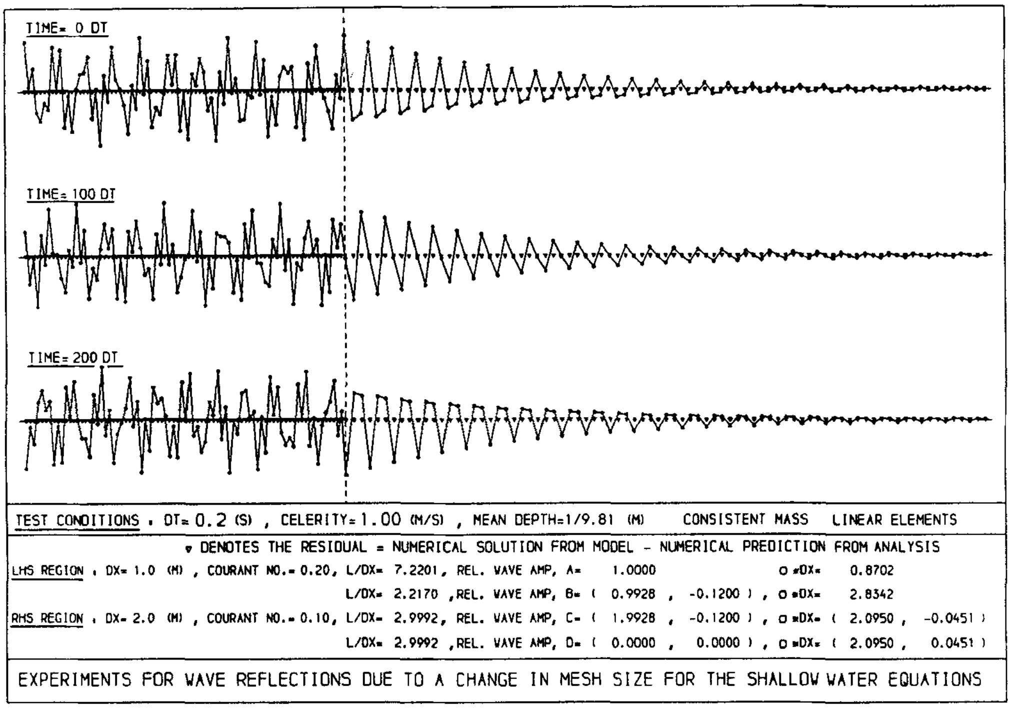

```
TEST CONDITIONS , DT= 0.2 (S) , CELERITY= 1.00 (M/S) , MEAN DEPTH=1/9.81 (M)    CONSISTENT MASS   LINEAR ELEMENTS
               ▾ DENOTES THE RESIDUAL = NUMERICAL SOLUTION FROM MODEL - NUMERICAL PREDICTION FROM ANALYSIS
LHS REGION , DX= 1.0 (M) , COURANT NO.= 0.20, L/DX= 7.2201, REL. WAVE AMP, A=   1.0000               o *DX=   0.8702
                                              L/DX= 2.2170 ,REL. WAVE AMP, B= ( 0.9928 , -0.1200 ) , o *DX=   2.8342
RHS REGION , DX= 2.0 (M) , COURANT NO.= 0.10, L/DX= 2.9992, REL. WAVE AMP, C= ( 1.9928 , -0.1200 ) , o *DX= ( 2.0950 , -0.0451 )
                                              L/DX= 2.9992 ,REL. WAVE AMP, D= ( 0.0000 ,  0.0000 ) , o *DX= ( 2.0950 ,  0.0451 )
EXPERIMENTS FOR WAVE REFLECTIONS DUE TO A CHANGE IN MESH SIZE FOR THE SHALLOW WATER EQUATIONS
```

Figure 9(a). Hot start numerical experiment—waves present: incident waves A ($7{\cdot}2201\Delta x_1$) and B ($2{\cdot}2170\Delta x_1$), and damped transmitted wave C

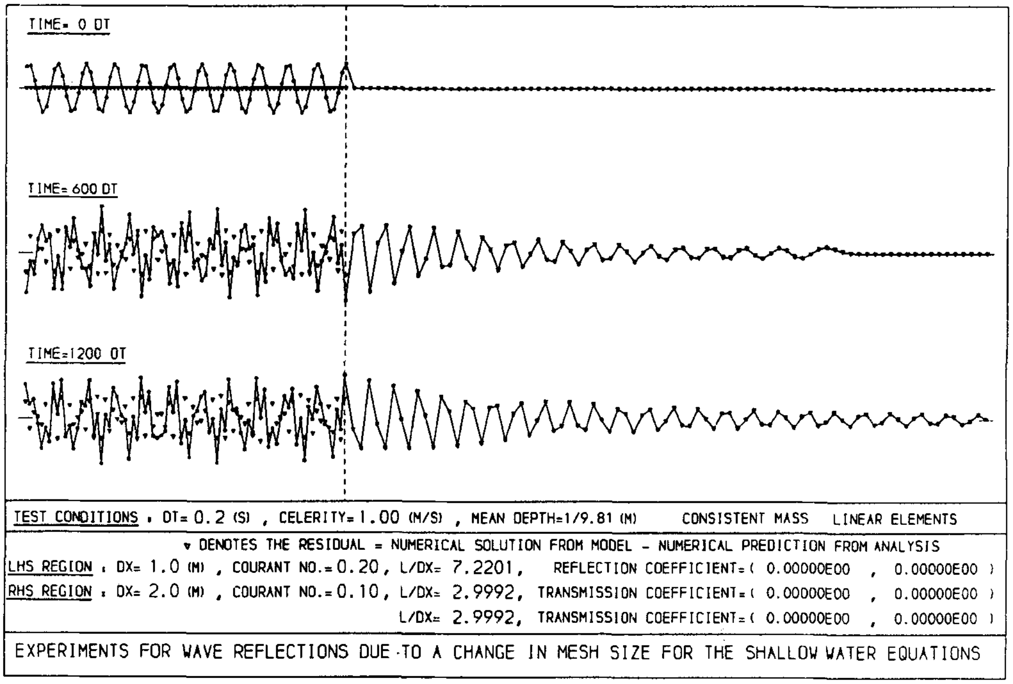

```
TEST CONDITIONS , DT= 0.2 (S) , CELERITY= 1.00 (M/S) , MEAN DEPTH=1/9.81 (M)      CONSISTENT MASS   LINEAR ELEMENTS
               ▾ DENOTES THE RESIDUAL = NUMERICAL SOLUTION FROM MODEL - NUMERICAL PREDICTION FROM ANALYSIS
LHS REGION , DX= 1.0 (M) , COURANT NO.= 0.20, L/DX= 7.2201,   REFLECTION COEFFICIENT= ( 0.00000E00  ,  0.00000E00 )
RHS REGION , DX= 2.0 (M) , COURANT NO.= 0.10, L/DX= 2.9992, TRANSMISSION COEFFICIENT= ( 0.00000E00  ,  0.00000E00 )
                                              L/DX= 2.9992, TRANSMISSION COEFFICIENT= ( 0.00000E00  ,  0.00000E00 )
EXPERIMENTS FOR WAVE REFLECTIONS DUE TO A CHANGE IN MESH SIZE FOR THE SHALLOW WATER EQUATIONS
```

Figure 9(b). Cold start numerical experiment with initially only the incident waves A ($7{\cdot}2201\Delta x_1$) present

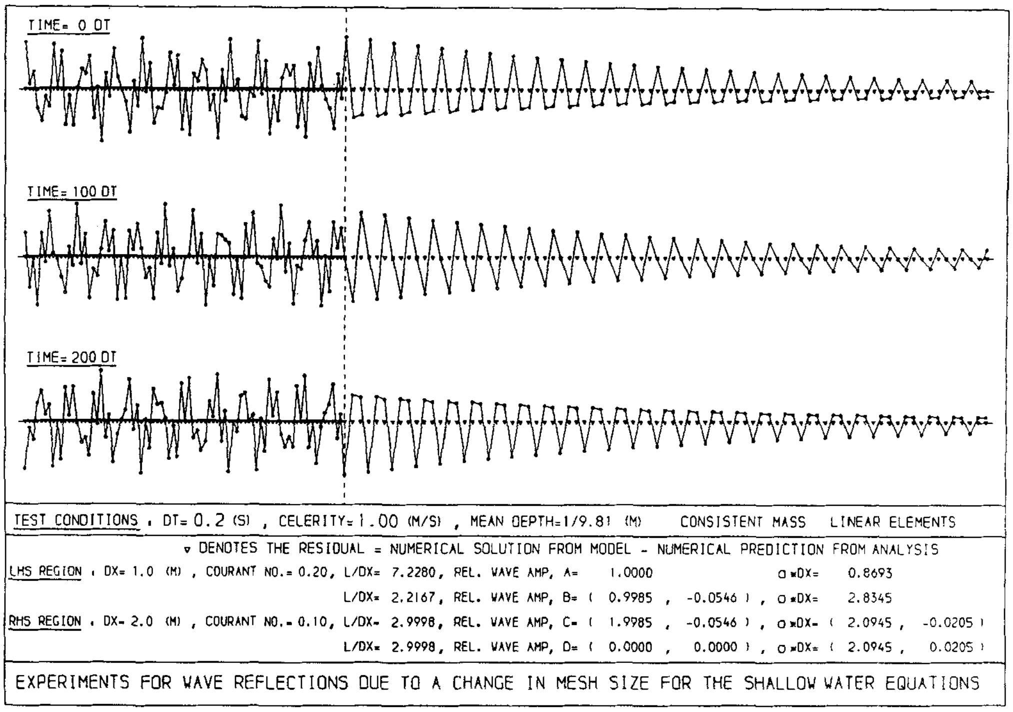

```
TEST CONDITIONS , DT= 0.2 (S) , CELERITY= 1.00 (M/S) , MEAN DEPTH=1/9.81 (M)     CONSISTENT MASS   LINEAR ELEMENTS
                  ▿ DENOTES THE RESIDUAL = NUMERICAL SOLUTION FROM MODEL - NUMERICAL PREDICTION FROM ANALYSIS
LHS REGION , DX= 1.0 (M) , COURANT NO.= 0.20, L/DX= 7.2280, REL. WAVE AMP, A=   1.0000                  σ*DX=   0.8693
                                              L/DX= 2.2167, REL. WAVE AMP, B= ( 0.9985 , -0.0546 ) , σ*DX=   2.8345
RHS REGION , DX- 2.0 (M) , COURANT NO.- 0.10, L/DX- 2.9998, REL. WAVE AMP, C- ( 1.9985 , -0.0546 ) , σ*DX- ( 2.0945 , -0.0205 )
                                              L/DX= 2.9998, REL. WAVE AMP, D= ( 0.0000 ,  0.0000 ) , σ*DX= ( 2.0945 ,  0.0205 )
EXPERIMENTS FOR WAVE REFLECTIONS DUE TO A CHANGE IN MESH SIZE FOR THE SHALLOW WATER EQUATIONS
```

Figure 10(a). Hot start numerical experiment—waves present: incident waves A (7·2280Δx_1) and B (2·2167Δx_1), and damped transmitted wave C

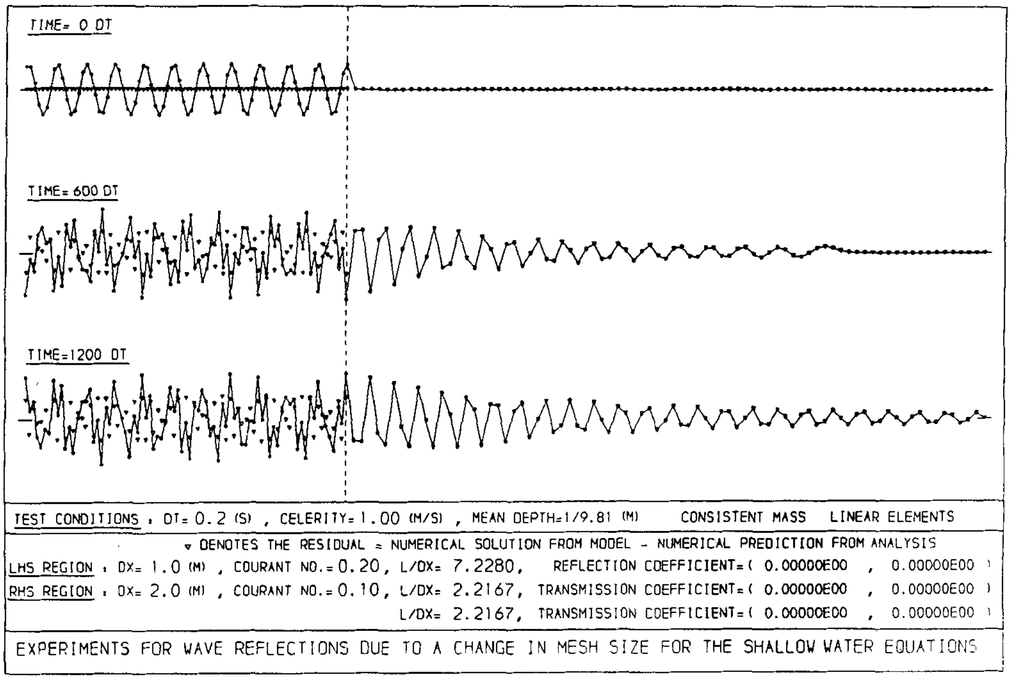

```
TEST CONDITIONS , DT= 0.2 (S) , CELERITY= 1.00 (M/S) , MEAN DEPTH=1/9.81 (M)     CONSISTENT MASS   LINEAR ELEMENTS
                  ▿ DENOTES THE RESIDUAL = NUMERICAL SOLUTION FROM MODEL - NUMERICAL PREDICTION FROM ANALYSIS
LHS REGION , DX= 1.0 (M) , COURANT NO.= 0.20, L/DX= 7.2280,   REFLECTION COEFFICIENT= ( 0.00000E00 , 0.00000E00 )
RHS REGION , DX= 2.0 (M) , COURANT NO.= 0.10, L/DX= 2.2167, TRANSMISSION COEFFICIENT= ( 0.00000E00 , 0.00000E00 )
                                              L/DX= 2.2167, TRANSMISSION COEFFICIENT= ( 0.00000E00 , 0.00000E00 )
EXPERIMENTS FOR WAVE REFLECTIONS DUE TO A CHANGE IN MESH SIZE FOR THE SHALLOW WATER EQUATIONS
```

Figure 10(b). Cold start numerical experiment with initially only the incident waves A (7·72280Δx_1) present

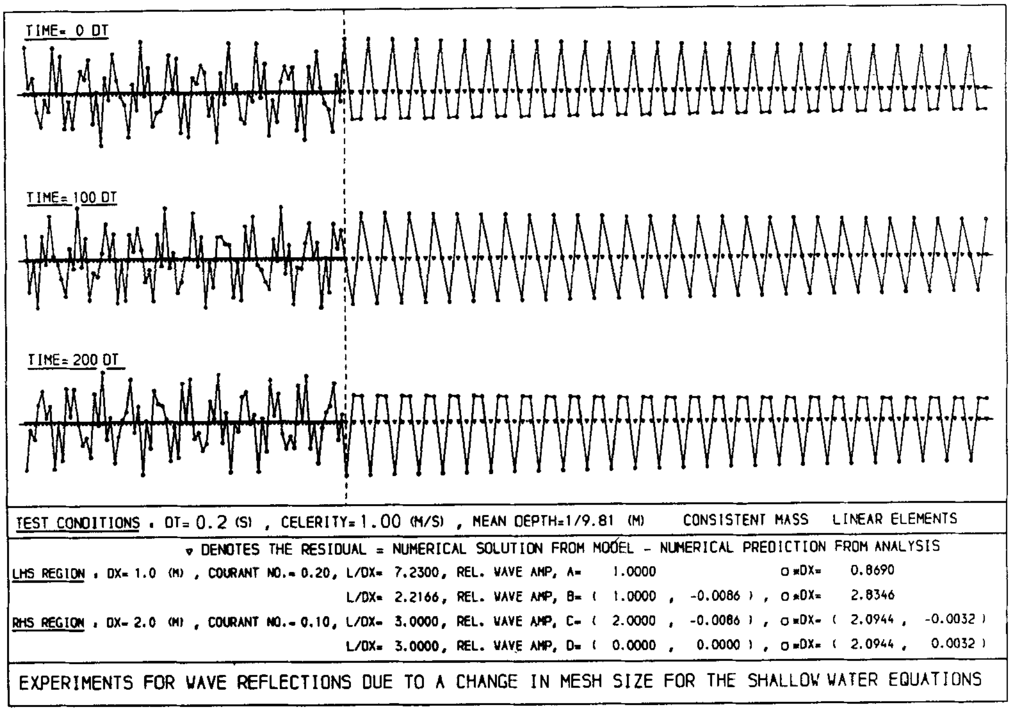

```
TEST CONDITIONS , DT= 0.2 (S) , CELERITY= 1.00 (M/S) , MEAN DEPTH=1/9.81 (M)    CONSISTENT MASS   LINEAR ELEMENTS
                 ▾ DENOTES THE RESIDUAL = NUMERICAL SOLUTION FROM MODEL - NUMERICAL PREDICTION FROM ANALYSIS
LHS REGION , DX= 1.0 (M) , COURANT NO.= 0.20, L/DX= 7.2300, REL. WAVE AMP, A=   1.0000                σ*DX=   0.8690
                                              L/DX= 2.2166, REL. WAVE AMP, B= ( 1.0000 ,  -0.0086 ) , σ*DX=   2.8346
RHS REGION , DX= 2.0 (M) , COURANT NO.= 0.10, L/DX= 3.0000, REL. WAVE AMP, C= ( 2.0000 ,  -0.0086 ) , σ*DX= ( 2.0944 , -0.0032 )
                                              L/DX= 3.0000, REL. WAVE AMP, D= ( 0.0000 ,   0.0000 ) , σ*DX= ( 2.0944 ,  0.0032 )
EXPERIMENTS FOR WAVE REFLECTIONS DUE TO A CHANGE IN MESH SIZE FOR THE SHALLOW WATER EQUATIONS
```

Figure 11(a). Hot start numerical experiment—waves present: incident waves A ($7{\cdot}2300\Delta x_1$) and B ($2{\cdot}2166\Delta x_1$), and damped transmitted wave C

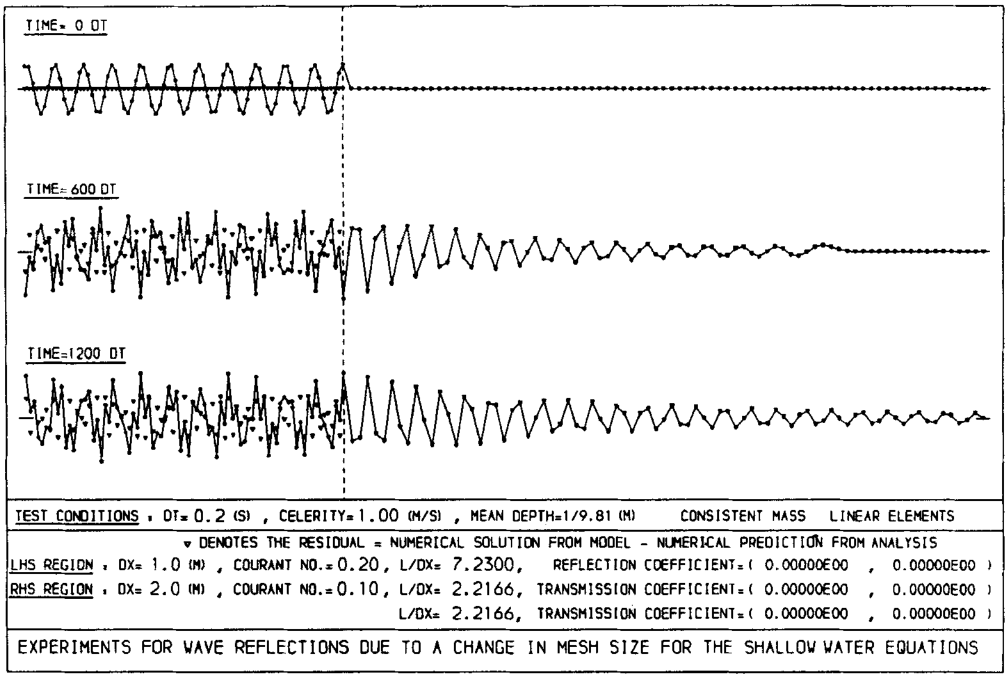

```
TEST CONDITIONS , DT= 0.2 (S) , CELERITY= 1.00 (M/S) , MEAN DEPTH=1/9.81 (M)     CONSISTENT MASS   LINEAR ELEMENTS
                 ▾ DENOTES THE RESIDUAL = NUMERICAL SOLUTION FROM MODEL - NUMERICAL PREDICTION FROM ANALYSIS
LHS REGION , DX= 1.0 (M) , COURANT NO.= 0.20, L/DX= 7.2300,   REFLECTION COEFFICIENT= ( 0.00000E00 , 0.00000E00 )
RHS REGION , DX= 2.0 (M) , COURANT NO.= 0.10, L/DX= 2.2166, TRANSMISSION COEFFICIENT= ( 0.00000E00 , 0.00000E00 )
                                              L/DX= 2.2166, TRANSMISSION COEFFICIENT= ( 0.00000E00 , 0.00000E00 )
EXPERIMENTS FOR WAVE REFLECTIONS DUE TO A CHANGE IN MESH SIZE FOR THE SHALLOW WATER EQUATIONS
```

Figure 11(b). Cold start numerical experiment with initially only the incident waves A ($7{\cdot}2300\Delta x_1$) present

Table I. Test data for the numerical experiments with an evanescent transmitted wave (C)

Test 1

$L_A/\Delta x_1 = 3{\cdot}0000$
$L_B/\Delta x_1 = 3{\cdot}0000$
$R(L_C/\Delta x_2) = 2{\cdot}5879$
$\gamma_C = 2{\cdot}4279 - i(0{\cdot}9730)$
$A = 1$
$B = -1 + 0i$
$C = 0 + 0i$
(see Figure 5(a))

Test 2

$L_A/\Delta x_1 = 3{\cdot}0100$
$L_B/\Delta x_1 = 2{\cdot}9901$
$R(L_C/\Delta x_2) = 2{\cdot}5880$
$\gamma_C = 2{\cdot}4279 - i(0{\cdot}9729)$
$A = 1$
$B = -1 - 0{\cdot}0093i$
$C = 0 - 0{\cdot}0093i$
(see Figure 6(a))

Test 3

$L_A/\Delta x_1 = 4{\cdot}0000$
$L_B/\Delta x_1 = 2{\cdot}5152$
$R(L_C/\Delta x_2) = 2{\cdot}6667$
$\gamma_C = 2{\cdot}3562 - i(0{\cdot}8814)$
$A = 1$
$B = -0{\cdot}7778 - i(0{\cdot}6285)$
$C = 0{\cdot}2222 - i(0{\cdot}6285)$
(see Figure 7(a))

Test 4

$L_A/\Delta x_1 = 7{\cdot}0000$
$L_B/\Delta x_1 = 2{\cdot}2255$
$R(L_C/\Delta x_2) = 2{\cdot}9802$
$\gamma_C = 2{\cdot}1083 - i(0{\cdot}2185)$
$A = 1$
$B = 0{\cdot}8355 - i(0{\cdot}5495)$
$C = 1{\cdot}8355 - i(0{\cdot}5495)$
(see Figure 8(a))

Test 5

$L_A/\Delta x_1 = 7{\cdot}2201$
$L_B/\Delta x_1 = 2{\cdot}2170$
$R(L_C/\Delta x_2) = 2{\cdot}9992$
$\gamma_C = 2{\cdot}0950 - i(0{\cdot}0451)$
$A = 1$
$B = 0{\cdot}9928 - i(0{\cdot}1200)$
$C = 1{\cdot}9928 - i(0{\cdot}1200)$
(see Figure 9(a))

Test 6

$L_A/\Delta x_1 = 7{\cdot}2280$
$L_B/\Delta x_1 = 2{\cdot}2167$
$R(L_C/\Delta x_2) = 2{\cdot}9998$
$\gamma_C = 2{\cdot}0945 - i(0{\cdot}0205)$
$A = 1$
$B = 0{\cdot}9985 - i(0{\cdot}0546)$
$C = 1{\cdot}9985 - i(0{\cdot}0546)$
(see Figure 10(a))

Test 7

$L_A/\Delta x_1 = 7{\cdot}2300$
$L_B/\Delta x_1 = 2{\cdot}2166$
$R(L_C/\Delta x_2) = 3{\cdot}0000$
$\gamma_C = 2{\cdot}0944 - i(0{\cdot}0032)$
$A = 1$
$B = 1 - i(0{\cdot}0086)$
$C = 2 - i(0{\cdot}0086)$
(see Figure 11(a))

amount of energy has leaked into the downstream region after $600\Delta t$ and $1200\Delta t$, but this is due to the fact that there are other Fourier components present in the initial set-up. These other components are due to the wave packet being semi-infinite.

With only a slight increase in incident wavelength to $3{\cdot}01\Delta x_1$ for the second test (see Figure 6(b)) there is little change in the results.

In the third test (see Figure 7(b)) a small but persistent damped wave is visible in region 2, even after some energy has leaked through the interface, which is to be seen after $600\Delta t$ as a long low-amplitude wave packet. The similarity between the 'hot'- and 'cold'-start tests is clear from a comparison of Figures 7(a) and 7(b).

Figures 8(b)–11(b) contain the results of the remaining 'cold-start' tests. After $1200\Delta t$ the resulting waveforms bear a reasonable resemblance to those in the 'hot-start' tests. If these tests could have been run for a longer duration, it is likely that the similarity in the waveforms between the two sets of tests would have become more marked. The reason that the last few tests require a longer run time is that the wavelength in region 2 is close to a $3{\cdot}0\Delta x_2$ wave, which is characterized by a zero group velocity and therefore requires a longer time to establish itself.

6. ENERGY FLUX BALANCE

In Section 3 the *complex* wave amplitudes B and C were calculated in terms of the incident wave amplitude A. If wave A has unit amplitude, then B and C are given by

$$B=\frac{E_{\mathrm{A}}-E_{\mathrm{C}}}{E_{\mathrm{A}}+E_{\mathrm{C}}}, \tag{28}$$

$$C=\frac{2E_{\mathrm{A}}}{E_{\mathrm{A}}+E_{\mathrm{C}}}, \tag{29}$$

where

$$E_{\mathrm{A}}=\frac{1+2\cos\gamma_{\mathrm{A}}}{2+\cos\gamma_{\mathrm{A}}}, \tag{26}$$

$$E_{\mathrm{C}}=\frac{1+2\cos\gamma_{\mathrm{C}}}{2+\cos\gamma_{\mathrm{C}}}, \tag{27}$$

$$\gamma_{\mathrm{C}}=\tan^{-1}\left(\frac{-1}{R_{\mathrm{A}}}\right)+\mathrm{i}\cosh^{-1}\left(\frac{2R_{\mathrm{A}}}{\sqrt{(1+R_{\mathrm{A}}^2)}}\right), \tag{30}$$

$$R_{\mathrm{A}}=\frac{H'\sin\gamma_{\mathrm{A}}}{2+\cos\gamma_{\mathrm{A}}}. \tag{31}$$

Since γ_{C} is complex, B and C will also be complex. This indicates the existence of a phase shift in waves B and C with respect to the incident wave A. The energy flux is given by the product of energy density and group velocity (see equations (50) and (51) of Part I) and for wave A this is given by

$$\begin{aligned} E_{\mathrm{flux\ A}}&=\left[\frac{\rho c^2A^2}{6h^2}(2+\cos\gamma_{\mathrm{A}})\right]\left[3c\cos^2(\omega\Delta t)\frac{1+2\cos\gamma_{\mathrm{A}}}{(2+\cos\gamma_{\mathrm{A}})^2}\right]\\ &=\left(\frac{\rho c^3\,1^2}{2h^2}\right)1^2\cos^2(\omega\Delta t)\,E_{\mathrm{A}}. \end{aligned} \tag{39}$$

Similarly for wave B,

$$\begin{aligned} E_{\mathrm{flux\ B}}&=\left(\frac{\rho c^3}{2h^2}\right)|B|^2\cos^2(\omega\Delta t)\,E_{\mathrm{B}}\\ &=\left(\frac{\rho c^3}{2h^2}\right)|B|^2\cos^2(\omega\Delta t)(-E_{\mathrm{A}}), \end{aligned} \tag{40}$$

where equation (26) has been used.

A comparison of equations (39) and (40) shows that the energy fluxes associated with waves A and B are equal and opposite if $|B|=1$, and this will now be proven.

In equation (28), since E_{A} is real and $E_{\mathrm{C}}=a+\mathrm{i}b$ (say) is complex, B can be expressed as

$$B=\frac{E_{\mathrm{A}}-(a+\mathrm{i}b)}{E_{\mathrm{A}}+(a+\mathrm{i}b)}. \tag{41}$$

If $|B|=1$ in equation (41), then E_A and/or 'a' equals zero. Since E_A is not generally zero, then $a=0$ and this implies that E_C would be purely imaginary. The truth of this can now be checked.

Letting $\gamma_C=\gamma_r+i\gamma_i$, then

$$E_C=\frac{1+2\cos\gamma_i}{2+\cos\gamma_i}=\frac{1+2(\cos\gamma_r\cosh\gamma_i+i\sin\gamma_r\sinh\gamma_i)}{2+\cos\gamma_r\cosh\gamma_i+i\sin\gamma_r\sinh\gamma_i}. \tag{42}$$

Inserting equations (9)–(11) into equation (42) and simplifying gives

$$E_C=i\sqrt{(3R^2-1)},$$

where

$$R=\left(\frac{2}{3\not{C}_2}\right)\tan\left(\frac{\omega\Delta t}{2}\right).$$

Since E_C is purely imaginary, $|B|=1$ and the energy fluxes due to waves A and B are equal and opposite. This means that if the energy fluxes balance across the interface, then the spatially damped wave C has zero energy flux associated with it.

7. GENERAL CONCLUSIONS

It has been demonstrated by analysis and experiment that if an incident wave (A) which has a wavelength in the range

$$3\cdot 0<\frac{L_A}{\Delta x_1}<\frac{\pi}{\tan^{-1}\{\sqrt{3}[H'-\sqrt{(H'^2-1)}]\}}$$

impinges on the interface of a mesh expansion, then an evanescent wave (C) will result in the downstream region. This wave is characterized by a complex wave number as well as a complex amplitude. The third wave present in the system is a short-wavelength wave (B) in the upstream region, which is incident in terms of phase but reflected in terms of energy (since it has a negative group velocity). This wave has a real wave number but a complex amplitude. The two incident waves in region 1 have complementary wave numbers which are related by equation (38). The energy flux balance is maintained between the two waves A and B in region 1. If energy is conserved across the interface, the damped wave C in region 2 does not transmit energy.

ACKNOWLEDGEMENTS

The work which has been detailed in Parts I, II and III was supported partly by the Consortium of North West Universities for Marine Technology, England and the Science and Engineering Research Council. Both organizations are gratefully acknowledged together with Dr. Brian Worthington (formerly of Hydraulics Research Pty. Ltd.) for some very helpful discussions, Lynne Hatcher for her excellent typing and the reviewer of these three papers.

REFERENCES

1. B. Cathers, S. Bates and B. A. O'Connor, 'Internal wave reflections and transmissions arising from a non-uniform mesh. Part I: An analysis for the Crank–Nicolson linear finite element scheme', *Int. j. numer. methods fluids*, **9**, 783–810 (1989).
2. B. Cathers, S. Bates, R. Penoyre and B. A. O'Connor, 'Internal wave reflections and transmissions arising from a non-uniform mesh. Part II: A generalized analysis for the Crank–Nicolson linear finite element scheme', *Int. j. numer. methods fluids*, **9**, 811–832 (1989).
3. T. J. Weare, 'Damping in "un-damped" finite difference representations', *J. Inst. Math. Appl.* **23**, 89–96 (1979).